Research Article

Green synthesis of single phase hausmannite Mn_3O_4 nanoparticles via *Aspalathus linearis* natural extract

A. Diallo[1,2,3,4] · N. Tandjigora[2,3] · S. Ndiaye[3,4] · Tariq Jan[5] · I. Ahmad[2,6] · M. Maaza[2,3]

Received: 28 September 2020 / Accepted: 31 March 2021

Published online: 17 April 2021

Abstract

Nowadays, green synthesis of nanoparticles using plant precursors has been extensively studied. However, less attention has been given to Mn_3O_4. This contribution validates the synthesis of single-phase Hausmannite Mn_3O_4 nanoparticles by a green approach without using any standard acid/base compounds, surfactants, and organic/inorganic dissolving agents. The chemical chelation of the Mn precursor was performed via bioactive compounds of the *Aspalathus Linearis'* extract, an African indigenous plant. Annealing at 400 °C for ~ 1 h was required to crystallize the small amorphous nanoparticles with an initial bimodal size distribution peaking at $\langle\phi_1\rangle \sim 4.21$ nm and $\langle\phi_2\rangle \sim 8.51$ nm respectively. Such annealing lead to increase in the diameter of the nanoparticles from 17 to 28 nm.The morphological, structural, vibrational, surface, and photoluminescence properties of the single-phase Hausmannite nanoparticles were comprehensively investigated by High Resolution Transmission Electron Microscopy(HRTEM),Energy Dispersive X-ray Spectroscopy (EDS), X-ray Diffraction (XRD), Raman and X-rays Photoelectron Spectroscopy (XPS), spectroscopy as well as room temperature photoluminescence. Structural and morphological investigations revealed the formation of quasi-spherical nanoparticles having a single phase Hausmannite Mn_3O_4 crystal structure. XPS results also validated the XRD results about the formation of Hausmannite Mn_3O_4 nanoparticles. Raman investigations allowed a crystal-clear distinction between the Mn_3O_4 nature of the nanoparticles from the potential γ -Mn_2O_3 phase as both phases belong to the same space group and both assume tetragonally-distorted cubic lattices of nearly similar dimensions. The optical studies of the single phase Hausmannite crystalline nanoparticles exhibited a broad photoluminescence in the spectral range of 300–700 nm, which is ideal for emission devices.

✉ A. Diallo, abdoulayediallosn@gmail.com | [1]Department of Physics and Chemistry, Faculty of Sciences and Technologies of Formation and Education, Cheikh Anta Diop University, Boulevard Habib Bourguiba, 5036 Dakar-Fann, Senegal. [2]UNESCO-UNISA Africa Chair in Nanosciences-Nanotechnology, College of Graduate Studies, University of South Africa, Muckleneuk ridge, PO Box 392, Pretoria, South Africa. [3]Nanosciences African Network (NANOAFNET), iThemba LABS-National Research Foundation, 1 Old Faure road, Somerset West, PO Box 722, Somerset West 7129, Western Cape, South Africa. [4]Groupe de Physique du Solide et Science des Matériaux, Department of Physics, Faculty of Sciences and Techniques, Cheikh Anta Diop University, 5005 Dakar-Fann, Senegal. [5]Physics Department, Allama Iqbal Open University, Islamabad, Pakistan. [6]NPU-NCP Joint International Research Center on Advanced Nanomaterials and Defects, Northwestern Polytechnical University, Xi'an, China.

SN Applied Sciences (2021) 3:562 | https://doi.org/10.1007/s42452-021-04550-3

Graphic abstract

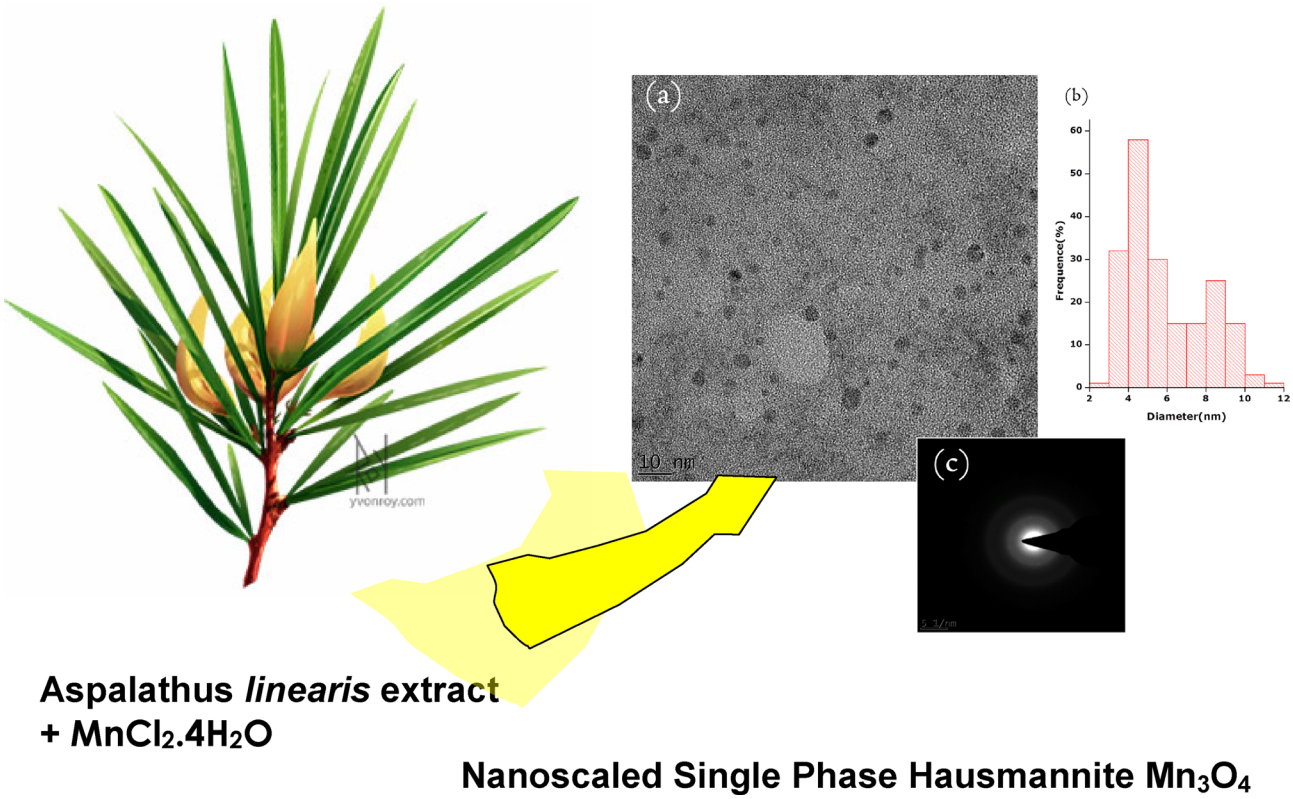

Keywords Green synthesis · Nanoparticles · Manganese oxide · Hausmannite · Mn_3O_4

1 Introduction

The Manganese oxide system exhibits a rich range of stoichiometric and crystallographic phases including β-MnO_2, γ-MnO_2, α-Mn_2O_3, γ-Mn_2O_3, α-Mn_3O_4, andMn_5O_8 where the Manganese atoms are obtained in different oxidation states. While burned in the air, such MnOx compounds undergo various electronic and/or crystallographic phase transformations. In the heat ranging from 500–600 °C, MnO_2 is converted to Mn_2O_3 and to Mn_3O_4 above 890 °C [1]. Depending on the environment, Mn may expect low or high oxidation states. The capacity to change within such oxidation states together with defects allows the well-established oxygen storage capacity of Mn oxides [2]. Manganese oxides in general and MnO, MnO_2, and Mn_3O_4 especially are attractive systems with potential applications in microwave absorption materials, sensors, supercapacitors, anode materials, water splitting and antimicrobial therapeutics [3–5]. Mn_3O_4 could potentially be employed as precursors for the synthesis of $LiMn_2O_4$ which is used for battery manufacturing. Also, Mn_3O_4 is known to be an efficient catalyst for the decomposition of waste gas of NOx [6]. Manganese oxide has been used as a raw material for fertilizer and as a mineral supplementation in animal feed for pharmaceutics in recent years. Synthesizing high-quality nanoparticles and researching the relationship between characteristics, size, and morphology is one of the keys to realizing these applications. As a result, scientists are constantly coming up with new preparation methods. Relatively to the most common Manganese oxide phases i.e. Pyrolusite MnO_2, Bixbyite Mn_2O_3, and Manganosite $Mn_{1-x}O$, the Hausmannite Mn_3O_4 is a high-temperature most stable phase. More precisely, it is generally produced by elevated calcination temperature above 1000 °C. Consequentially, the investigation of the low-temperature routes for the synthesis of the Hausmannite Mn_3O_4 is of a special interest. Few attempts to synthesize Mn_3O_4 at low temperature regimes are reported in the literature. Among the explored routes, two have been found promising: sol–gel processing of Manganese alkooxides, and controlled oxidation of aqueous suspensions of $Mn(OH)_2$. The synthesis mechanism of Mn_3O_4 could be classified into two principal groups. The primary group is the oxidative pyrolysis of manganese

Table 1 Some details of synthesis procedures of Mn3O4 nanoparticles

Synthesis method	Synthesis temp. (°C)	Synthesis time (h)	Precursor materials	Particles size (nm)	ref
Calcination method	800	3	$Mn(CH_3COO)_2.4H_2O$, Mn(acetylacetonate) and egg white	60	[7]
Thermal method	260	1	Bis(2-hydroxy-1 naphthaldehydato) manganese(II)	9–24	[8]
Solvothermal method	160	24	MnCl2, NaOH and 1, 10-phenanthroline	60	[9]
Refluxing method	100	4	Mn hydroxide and gel	50	[10]
Hydrothermal method	200	24	$Mn(NO_3)_2$ sol. (50 wt%)	26	[11]
Selfassembly method	60	24	$KOH–C_2H_5OH$ &Mn(CH3COO)2. $4H_2O–C_2H_5OH$,	5.5	[12]
Gas–liquid reaction	50	~0.1	$Mn(CH_3COO)_2$ $4H_2O$, Ethanol and $NH_3{\cdot}H_2O$ (25–28 wt%)	24.4	[13]
Microwave Irradiation	80	≤0.1	Manganese nitrate, ethanolamine, ethylenediamine and ethanol	10	[14]

salts, for instance, the calcination and the thermal decomposition methods [7, 8]. These methods require expensive manganese precursors and are also energy waste intensive. The second category is the oxidation of intermediate manganese hydroxide ($Mn(OH)_2$), such as solvothermal, refluxing, hydrothermal, and the self-assembly methods [9–12].Yet cost effective, these processes are relatively time consuming in general. This is because the Mn_3O_4 nanoparticles are achieved through a low dynamic gas–solid reaction within O_2 and $Mn(OH)_2$. As summarized in Table 1, yet very effective, the bulk of physical and chemical routes to synthesize Mn_3O_4 nanoparticles seem not be green processes in regard of the rules of green chemistry. There are many physical and chemical methods for synthesis of nanoscale materials, but the ones that use green chemistry and eco-friendly techniques are the most suitable. The synthesis of nanoparticles using green technologies is highly needed for the rapid translation of nanostructures to real-world applications [5, 15].This is because the process of formation of the nanoparticles does not require any toxic stabilizing, reducing, and oxidizing agents and can be done under ambient temperature and pressures. Three

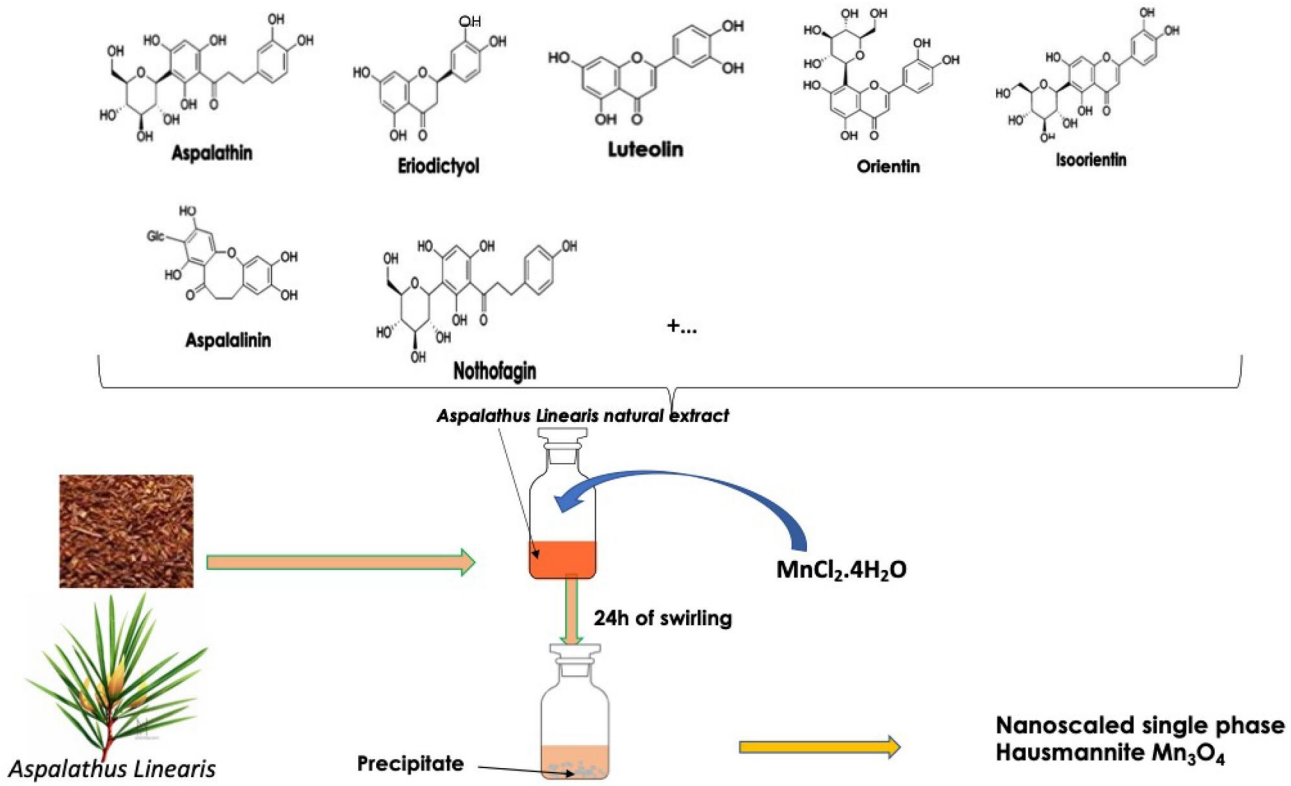

Fig. 1 A schematic diagram of a possible mechanism for the formation of nanoparticles by Aspalathus linearis extract

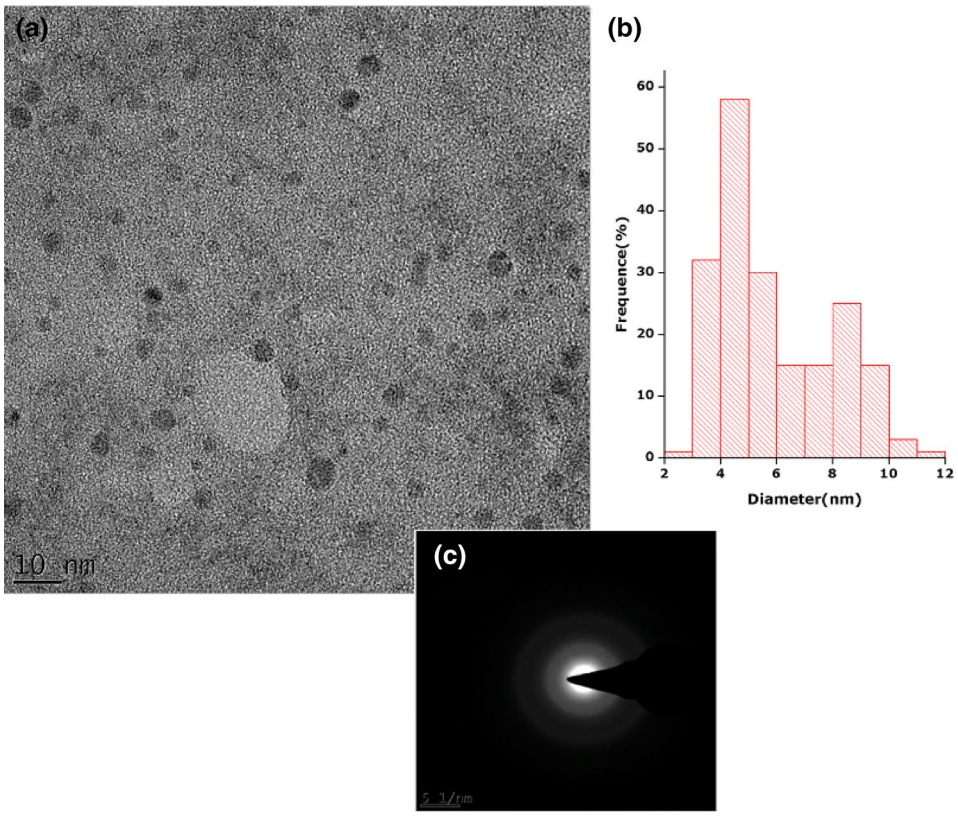

Fig. 2 HRTEM of the Manganese oxide nanoparticles with size-frequency and SAED

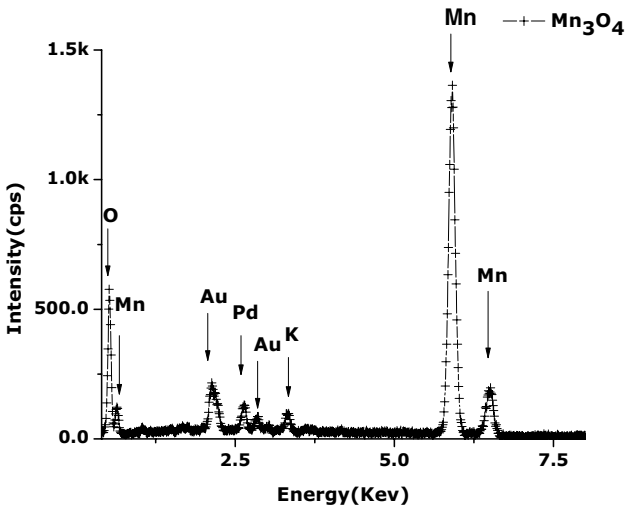

Fig. 3 EDS spectrum of the Manganese oxide nanoparticles synthesis nanoparticles at 400 °C

methods of green synthesis using plant extracts, green synthesis using microorganisms, and lower-temperature synthesis have been explored for Mn_3O_4 and other nanoparticles green synthesis [16–19]. However, a very limited number of green synthesis methods using plant extracts as chelating agents have been reported. The plant extract can be used as a valuable source for bioreduction of metallic ions and nanoparticle development because of its potent antioxidants [20]. Prasad [21] reported the green synthesis of Mn_3O_4 nanoparticles (44–66 nm) using *Adalodakam* leaf extract and NaOH. Asaikkutti [22] used *Ananas comosus (L.)* peel extract and ethanol in their experimental protocol to prepare Mn_3O_4 nanoparticles having a particle size of 40–50 nm. [23] utilized *Azadirachta Indica* leaf extract as a reducing and capping agent for the synthesis of Mn_3O_4 nanoparticles (18.2–30 nm) at 400 °C for 2 h. Synthesis of Mn_3O_4 nanoparticles (15 nm) at500 °C for 2 h using *Simarouba Glauca* leaf extract and ethanol, was reported by Sreekala et al. [24]. Yet economically of interest, compared to the traditional methods, which use toxic organic solvents or precursors, these processes are relatively energy-consuming in general.

Herein, single phase Hausmannite Mn_3O_4 nanoparticles are synthesized via *Aspalathus linearis* by a green approach. The process of formation of nano-scaled Mn_3O_4 particles does not require any standard acid/base compounds, neither surfactants nor organic/inorganic dissolving agents. As one could conclude later, it allows the synthesis of the ultrafine nanoparticles with an initial size distribution of 4.21–8.51 nm at the lowest temperature. The morphological, structural, vibrational, surface, and photoluminescence properties of the nano-scaled particles investigated by HRTEM, EDS, XRD, Raman, XPS, and PL are presented.

2 Materials and methods

2.1 Green synthesis of manganese oxide nanoparticles via *Aspalathus Linearis*

Aspalathus Linearis, known as Rooibos, is a plant native of Southern Africa which has great importance in the synthesis of nanoparticles. Its leave extract contains phenolic compounds with a higher anti-oxidant potential and, as a result, a significant metal ion reduction capacity, making green synthesis of nanoparticle possible. Additionally, the high protein, lipid, and amino acid content aids in the stabilization of nanoparticles growth while preventing agglomeration [25–27]. For the synthesis of Manganese oxide nanoparticles, 8 g powders of dried *A. linearis* leaves from its primary geographical region, i.e. the Cederberg region-South Africa, were cleaned and added to 300 ml of de-ionized water at Room Temperature for 48 h. The filtrated solution was mixed with 3 g of $MnCl_2.4H_2O$ (Sigma-Aldrich, purity 99.99%) as a demonstration of the idea of green synthesis of Hausmannite Mn_3O_4 nanoparticles at low temperatures and by an entirely green process. As swirling the solution, the precursor was seen to dissolve entirely in the solution, provoking a color turn from brown to greyish-brown. Following such a phase, a gray colored precipitate (Presumably MnO and/or Mn (OH)2 based mixture) was observed throughout 48 h. The precipitates were collected and dried at ~ 100 °C to remove any extra water content. Figure 1 depicts a schematic diagram of a potential mechanism for *A. linearis* extract-induced nanoparticle formation. In the formation of the nanoparticles, the plant extract acts as a reducing agent as well as a capping or binding agent. However, the interpretation and final chemical reactions taking place are expected to be challenging.The nanoparticles were annealed in air at 400 °C for 1 h to induce their crystallization, as described in Sect. 3.

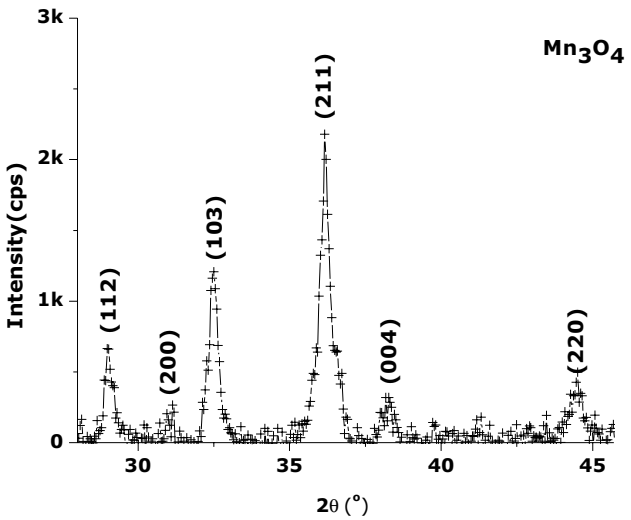

Fig. 4 XRD spectrum of the Manganese oxide nanoparticles synthesis nanoparticles at 400 °C

2.2 Characterization techniques

Various characterizations were conducted to study various properties of the synthesized nanoparticles. For morphology and electron microscopy investigations the HRTEM, a Jeol JEM 4000EX electron microscopy unit with a resolution limit of about 0.12 nm, equipped with a Gatan digital camera, was utilized. The EDS spectrum was collected with an Oxford instruments X-Max solid-state Silicon drift detector operating at 20 keV. The structural properties of the annealed nanoparticles were characterized by using XRD Model Bruker AXS D8 Advance using radiation of Cu (K_α Having wavelength of 1.5406 Å) and a Jobin–Yvon-SPEX integrated Raman spectroscopy with excitation wavelength of 632.8 nm. For the XPS, a VG Scientific LAB MK-II spectrometer with an Mg–Ka X-ray source (1253.6 eV) was used. The photoluminescence properties were analyzed at 250 nm using Horiba Jobin Yvon Fluorolog III modular spectrofluorometer.

Table 2 X-ray diffraction parameters and extracted nanoparticles' characters

(hkl)	θ_{exp} (rad)	d_{hkl}^{Exp} (Å)	d_{hkl}^{Bulk} (Å)	$\Delta d_{hkl} / d_{hkl}^{Bulk}$ (%)	FWHM (rad)	$\langle\phi_{particle}$ (nm)	Sizeaverage $\langle\phi_{particle}$ (nm)	$\langle a^{Exp}$ (Å)	$\langle c^{Exp}$ (Å)
(112)	0.253	3.077	3.089033	– 5.0	0.3149	26.05	23.70	5.756	9.406
(200)	0.271	2.878	2.880995	– 1.0	0.2972	27.74			
(103)	0.284	2.754	2.768005	– 1.9	0.3411	24.25			
(211)	0.316	2.481	2.486999	– 1.9	0.4129	20.24			
(004)	0.334	2.351	2.366977	– 4.7	0.3158	26.62			
(220)	0.388	2.086	2.036904	– 0.3	0.4807	17.85			

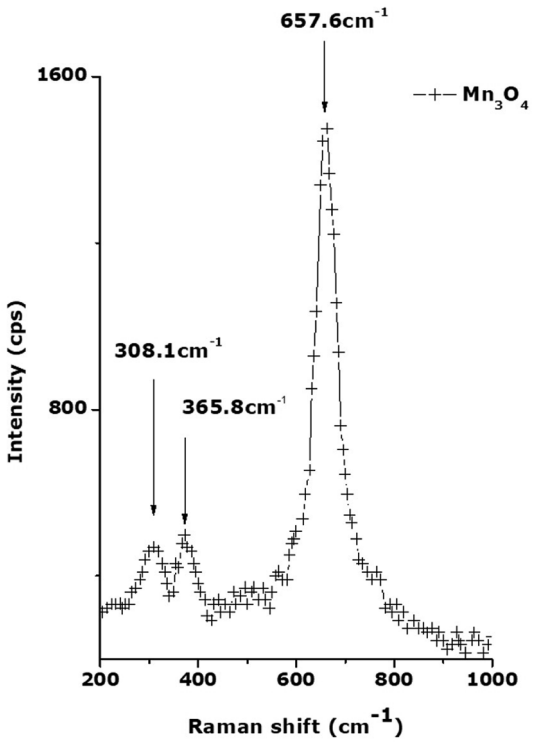

Fig. 5 Raman spectrum of the Manganese oxide nanoparticles synthesis nanoparticles at 400 °C

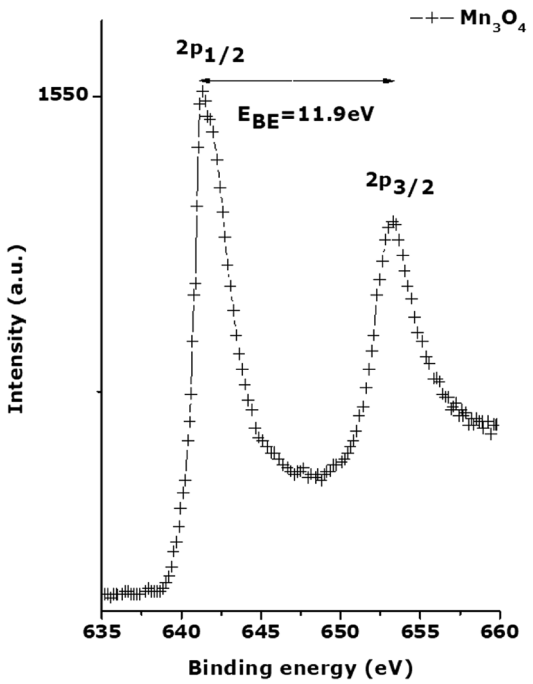

Fig. 6 XPS of the Hausmannite nanoparticles

3 Results and discussion

3.1 Morphology and electron microscopy investigations

Morphology of the un-annealed sample, i.e. the isolated precipitates dried at ~ 100 °C was analysed with the TEM**.** Figure 2a indicates that the dried precipitate consists of dispersed quasi-spherical nanoparticles. Following a digitization analysis from multiple TEM images, the nanoparticles' size was found to obey a bi-modal distribution with average diameters peaking at $\langle \phi_1 \rangle \sim 4.21$ nm and $\langle \phi_2 \rangle \sim 8.51$ nm respectively (Fig. 2b). Of those views in different areas of the sample, it was found that the initial dried precipitate consists of amorphous nanoparticles (Fig. 2c).

3.2 Elemental analysis

Figure 3 displays the EDS spectrum of the initial precipitates dried at ~ 100 °C. In addition to the expected peaks of Mn (0.63, 5.90 and 6.49 keV) and O (0.52 keV), 3 supplementary peaks matching Au, Pd and K can be seen. Except for the detected K (3.31 keV), the Au and Pd peaks originate both from the Au–Pd coating which was done to minimize surface electron charging via the EDS elemental investigations. The presence of Potassium can be related to the *Aspalathus linearis'*extract. The support for such a conclusion is justified by the high grade of the chemical Mn precursor (99.99% Sigma Aldrich) and the fact that all required precautions during the synthesis were considered. As no other elements were detected in the EDS spectrum, this suggests the chemical formation of an Mn_xO_y or a slightly hydrated phase such as MnO or $Mn(OH)_2$ respectively, but certainly no $MnCl_2$ as there is no trace of chlorine.

3.3 Structural and crystallographic analysis

Following the thermogravimetry and differential calorimetry preliminary investigations, it was found that a heat treatment above 371 °C is required to crystallize the initially amorphous Mn_xO_y. Hence, the initial precipitates were dried at ~ 100 °C and thereafter annealed at about 400 °C for 1 h. The duration of 1 h was the optimum time extent of annealing to avoid significant sintering. In terms of crystallographic structure, Hausmannite Mn_3O_4 exist into two forms: low-temperature tetragonal and high-temperature cubic structure by a transition happening at around 1170 ◦C [28]. Likewise, it is established that the cubic Mn_3O_4 structure stabilizes toward ambient temperature in films produced by MOCVD on single-crystal (100) MgO substrate [29]. Figure 4 exhibits an XRD pattern of the annealed nanoparticles (400 °C, 1 h) in air. The pattern of the annealed powder is indexed as pure Hausmannite

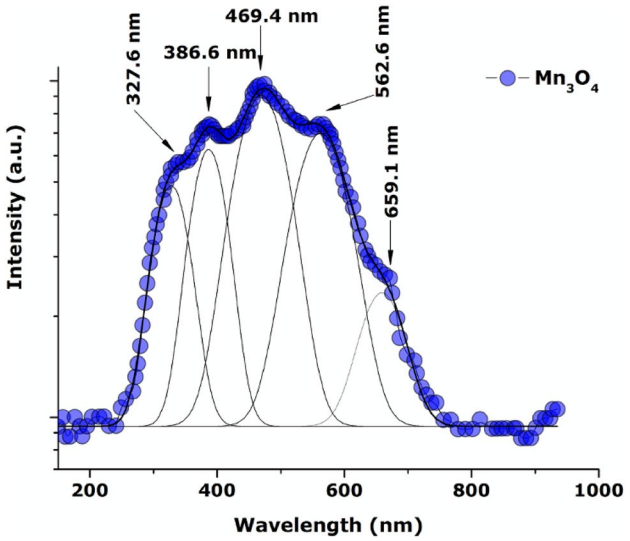

Fig. 7 Room Temperature PL of the Hausmannite nanoparticles

Mn_3O_4 structure with average values of lattice parameters $\langle a_{nano} \sim 5.756$ Å ($\langle a_{bulk} = 5.76210$ Å) and $\langle c_{nano} \sim 9.406$ Å ($\langle c_{bulk} = 9.46960$ Å) matching the Joint Committee on Powder Diffraction Standards (JCPDS) card no 24-0734 related to body-centered tetragonal Mn_3O_4 phase. These results are in good agreement with the green synthesis of Hausmannite Mn_3O_4 by [23, 30]. No additional Bragg peaks from pure Mn or other Mn–O phases have been detected (At least within the XRD detection limit).The relative Bragg peaks broadness means that the nanocrystalline nature of the tetragonal Mn_3O_4 powder is conserved in subsequent heat treatment. Debye Scherrer equation ($\langle \phi_{particles} \sim 0.9\,\lambda/(\Delta\theta_{1/2}\cos(\theta_B))$ permits estimating the medium diameter of the Mn_3O_4 nanocrystals $\langle \phi_{particles}$ which was found in the range 17–28 nm as listed in Table 2. Further, data in Table 2 reveals that the quotient $(d_{hkl}^{Exp}\text{-}d_{hkl}^{Bulk})/d_{hkl}^{Bulk}$ ranges between 5.0–0.3% each h,k,l indices. This variation suggests the existence of compressive strain in the annealed powder [31]. In fact, more accurate analysis of the JCPDS database shows that the pattern assignable to the tetragonal Hausmannite Mn_3O_4 can also be assigned to γ-Mn_2O_3 if one considers the bar-errors on the lattice parameters. If so, the XRD can not easily distinguish between Hausmannite Mn_3O_4 and γ-Mn_2O_3 because both materials belong to the same space group and both assume tetragonally-distorted cubic lattices of nearly similar dimensions. Consequentially, it is necessary to carry out at least Raman studies as the vibrational characteristics of the Hausmannite Mn_3O_4 and γ-Mn_2O_3 are indeed different.

3.4 Vibrational properties

Hausmannite belongs to the $I4_1/amd–D_{4h}^{19}$ space group with $Z = 4$ [32–35] for which the group theory predicts the vibrational representation of a primitive cell as $\Gamma_{D4h} = 2A_{1g}(R) + 2A_{1u}(IN) + A_{2g}(IN) + 4A_{1u}(IR) + 3B_{1g}(R) + 2B_{1u}(IN) + B_{2g}(R) + 4B_{2u}(IN) + 4E_g(R) + 6E_u(IR)$, where "*R*", "IR" and "IN" means Raman, IR, and inactive lattice vibrations. Following [32] vibrational spectra of Manganese oxides can be divided into 3 regions at 750–600, 600–450, and 450–200 cm^{-1}, where stretching, bending and wagging vibrations of Mn_xO_y units take place respectively. The most discernible modes in Raman are vibrations centered at 660, 370, and 318 cm^{-1}. As it was demonstrated in several forms of the tetragonal Hausmannite Mn_3O_4, i.e. bulk, thin films, nanocrystals, nanorods and nano-powdered forms, these are 3 main active Raman modes [6, 36–40]. Figure 5 reports the Raman spectrum of the nanoparticles (~ 400 °C, 1 h). As one could observe, it constitutes a relatively intense peak at 657.6 cm^{-1} and two smaller peaks centered at around 308.1 and 365.8 cm^{-1}. These three Raman bands are consistent with the green synthesis of Mn_3O_4 nanoparticles using plant precursor by [23]. The appearance of three Raman bands is attributed to the crystalline Hausmannite structure [41, 42] of greenly synthesized nanoparticles, without any other oxides phase. The three Raman band are ascribed to the A_{1g}, E_g, and T_{2g} respectively. The relatively intense Raman peak i.e., the A_{1g} (657.6 cm^{-1}) is the fingerprint of the Hausmannite with the spinel structure characterizing the unique Hausmannite Mn–O stretching vibrational mode of the Mn ions in the tetrahedral coordinating. If the positions of 3 Raman modes are compared to the bulk values of pure tetragonal Hausmannite Mn_3O_4, they are red-shifted. The corresponding shift is about 2.4, 4.2 and 9.9 cm^{-1} for 660, 370, and 318 cm^{-1} modes respectively. This shift can be assigned rather to a size effect than to an oxygen deficiency as reported by Zuo et al. in nano-scaled Mn_3O_4 particles synthesized by γ-radiolysis [40]. More precisely, as proposed by Zuo et al. and other researchers in their studies [43–45], the observed spectra can be explained by the phonon confinement effect. The phonon confinement model is based upon the fact that while in an infinite crystal, only phonons near the center of the Brillouin Zone i.e. $q \sim 0$ contribute to the Raman spectrum in view of the momentum conservation between phonons and probing light (Raman peaks are sharp), the phonons are confined in space by crystal boundaries or defects in a finite crystal such as nano-scaled particles ($\langle \phi_{particle} < \lambda_{Incident}$). This results in uncertainty in the phonon momentum, allowing phonons with q#0 to contribute to the Raman spectrum. This uncertainty is larger for smaller particles, and hence induces the red shift as well as the broadening of

the Raman peak. From this section, one can deduce that the synthesized Manganese oxide nanoparticles are not γ-Mn_2O_3 but pure Hausmannite Mn_3O_4 exhibiting a phonon confinement due to size effect.

3.5 Surface properties

To support the XRD and Raman studies, XPS investigations of annealed were conducted at room temperature. Figure 6 displays the XPS spectrum of synthesized nanoparticles (annealed at 400 °C for1 hour). More specifically, it describes the Mn_{2p} peaks and equivalent binding energies. The $2p_{1/2}$ and $2p_{3/2}$ are collected at 641.3 and 653.2 eV. The observed spin–orbit splitting is ~ 11.9 eV, which is in good comparison with that of Manganese oxides [14, 46]. The binding energy values from the Mn $2p_{3/2}$ (641.3 eV) and spin–orbit splitting (11.9 eV) were in good agreement with those related values of Manganese oxides. Thus, the XPS analysis confirms the Hausmannite Mn_3O_4 phase of the synthesized nanoparticles.

3.6 Photoluminescence properties

Figure 7 depicts the room temperature photoluminescence spectrum of the synthesized single-phase Hausmannite Mn_3O_4 nanoparticles using 250 nm excitation wavelength within the spectral range of 160–950 nm; under the conditions which are similar to those of [47]. One can distinguish five major emissions centered at 327.6, 386.6, 469.4, 562.6 and 659.1 nm with the following width at half maximum $\Delta_{1/2}$: 62.9, 61.9, 87.8, 92.5 and 77.4 nm respectively. Yet with slight spectral shift, this photoluminescence response is very close to that obtained by Toufiq et al. for hydrothermally-grown single-crystalline tetragonal Mn_3O_4 nanoparticles using similar Mn precursor $MnCl_2.4H_2O$ [47]. The UV emission bands located at 327.6 nm and 386.6 nm correspond to the recombination and emission of free excitons through an exciton–exciton collision process near band edges of the well crystallized crystals [48, 49]. The most intense blue emission collected at 469.4 nm could be ascribed to the radial recombination of the photo-generated hole with an electron resulting in singly ionized oxygen vacancy-related defects. The yellow emission located at 562.6 nm can be assigned to the d–d transitions involving Mn^{3+} ions [50]. The combined emission covering a large spectral range from the UV to NIR (300–700 nm) could be of interest for technological applications in ultraviolet and visible light emission devices.

As it is highlighted in Sect. 1, green synthesis using *Adalodakam leaf* extract and NaOH resulted in formation of nanocrystalline Mn_3O_4 (44–66 nm) (Prasad et al.). The XRD analysis confirmed the formation of Mn_3O_4 in a tetragonal body-centered lattice system. Asaikkuti et al. used *Ananas comosus (L.) peel* extract and ethanol to produce spherical Mn_3O_4 nanoparticles with average particle size of 40–50 nm for dietary supplementation. The formation of Mn_3O_4 nanoparticles was further validated by SEM and EDS. However, NaOH solutions can decompose proteins and lipids in living tissues, which consequently cause chemical burns and may induce permanent blindness upon contact with the eye. Ethanol can lead to malnutrition, and can exert a direct toxicological effect due to its interference with hepatic metabolism and immunological functions. [23] utilized *Azadirachta Indica* leaf extract as a reducing and capping agent for the green synthesis of Mn_3O_4 nanoparticles having particles size of (18.2–30 nm) annealed at 400 °C for 2 h. Synthesis of Mn_3O_4 nanoparticles (15 nm) at annealed at 500 °C for 2 h using *Simarouba Glauca* leaf extract and ethanol, was reported by Sreekala et al. However, in comparison to the above green protocol which uses harmful organic or inorganic precursors, these protocols are relatively energy-consuming. Obviously, the current green synthesis protocols characterization studies have many advantages over the previous works, such as the synthesis of ultrafine non-agglomerated nanoparticles having a size distribution of 4.21–8.51 nm at lower temperature, lower cost, use of *Aspalathus Linearis* extract, which possesses anti-oxidant, antiaging, anticancer, antidiabetic and anti-inflammatory properties [51]. In addition, the nano scaled feature of the synthesized particles was demonstrated by TEM, and XRD investigations, and the combined XRD, EDS, Raman, and XPS spectroscopy studies verified the nature and/or single-phase formation of the Mn_3O_4 nanoparticles.

Likewise, there is a need to identify the mechanism of the green synthesis and related various physical and chemical reactions so to derive a likely universal model of green synthesis of nano-oxides [52–60]. Also, it is expected to demonstrate this procedure for the green synthesis of other functional simple monoxides [61], bioxides [62, 63] and nanocomposites [64, 65].

Taking into the observed physical responses, and as a follow up study of the current nanoscale single phase Hausmannite, it is intended to carry out the following studies: UV response [66], hydrophobicity [63, 67], antibacterial [68] as well as their doping with rare earth elements [69, 70]. Likewise, the mechanism of the green synthesis will be investigated to identify the bioactive compounds involved in the chelation process [31, 52, 71].

4 Conclusions

It was demonstrated that pure and nano-scaled Hausmannite Mn_3O_4 can be synthesized by a green chemistry approach using *A. linearis* natural extract. Comparatively

to the literature, this process allows the synthesis of the smallest Hausmannite nanoparticles in size and prepared to lowest temperature. While the kinetics of their formation is relatively slow, their initial size distribution is bimodal, peaking at $\langle\phi_1 \sim 4.21$ nm and $\langle\phi_2 \sim 8.51$ nm respectively. An annealing at 400 °C for 1 h approximately is required to induce their crystallization which provokes a sintering phenomenon as their average diameter reaches 17–28 nm. The broad photoluminescence generated by the single phase Hausmannite crystalline nanoparticles in the 300–700 nm spectral range is ideal for emission devices. It is intended to carry out studies to shed-light on the mechanism of formation of such Hausmannite Mn_3O_4 nanoparticles and the evolution of their surface coordination. More precisely, it is hoped that the ongoing investigations will allow us to identify the bioactive compounds which react with the Mn precursor as well as the various chemical phases through which the reaction is taking place.

Funding This research output was supported by grants from the National Research Foundation of South Africa (NRF), iThemba LABS, the UNESCO-UNISA Africa Chair in Nanosciences and Nanotechnology, The World Academy of Sciences (TWAS), the Abdus Salam ICTP through the Nanosciences African Network (NANOAFNET) as well as the African Laser Centre (ALC) to whom we are grateful.

Declarations

Conflict of interest On behalf of all authors, the corresponding author states that there is no conflict of interest.

References

1. Reidies AH (1986). In: Elvers B, Hawkings S, Schulz G (eds) Ullmann's Encyclopedia of industrial chemistry. VCH, New York
2. Chang Y, McCarty JG (1996) Novel oxygen storage components for advanced catalysts for emission control in natural gas fueled vehicles. Catal Today 30:163–170. https://doi.org/10.1016/0920-5861(95)00007-0
3. Veeramani H, Aruguete D, Monsegue N, Murayama M, Dippon U, Kappler A, Hochella MF (2013) Low-temperature green synthesis of multivalent manganese oxide nanowires. ACS Sustain Chem Eng 9:1070–1074. https://doi.org/10.1021/sc400129n
4. Kumbhar VS, Lee H, Lee J, Lee K (2019) Recent advances in water-splitting electrocatalysts based on manganese oxide. Carbon Resour Convers 2(3):242-255. https://doi.org/10.1016/j.crcon.2019.11.003
5. Rahmat M, Rehman A, Rahmat BHN, Iqbal M, Khan WS, Jamil W, Sadia Bajwa SZ, Sarwar Y, Rasula S (2019) Laser ablation assisted preparation of MnO_2 nanocolloids from waste battery cell powder: Evaluation of physico-chemical, electrical, and biological properties. J Mol Struct 1191:284–290. https://doi.org/10.1016/j.molstruc.2019.04.094
6. Yang L, Zhu Y, Tong H, Wang W, Cheng G (2006) Low temperature synthesis of Mn_3O_4 polyhedral nanocrystals and magnetic study. J Solid State Chem 179:1225. https://doi.org/10.1016/j.jssc.2006.01.033
7. Durmus Z, Baykal A, Kavas H, Direkçi M, Toprak MS (2009) Ovalbumin mediated synthesis of Mn_3O_4. Polyhedron 11:2119–2122. https://doi.org/10.1016/j.poly.2009.03.026
8. Davar F, Salavati-Niasari M, Mir N, Saberyan K, Monemzadeh M, Ahmadi M (2010) Thermal decomposition route for synthesis of Mn_3O_4 nanoparticles in presence of a novel precursor. Polyhedron 29:1747–1753. https://doi.org/10.1016/j.poly.2010.02.026
9. Mehdizadeh R, Saghatforoush LA, Sanati S (2012) Solvothermal synthesis and characterization of α-Fe_2O_3 nanodiscs and Mn3O4 nanoparticles with 1,10-phenanthroline. Superlattice Microst 52:92–98. https://doi.org/10.1016/j.spmi.2012.03.017
10. Anilkumar M, Ravi V (2005) Synthesis of nanocrystalline Mn_3O_4 at 100 °C. Mater Res Bull. https://doi.org/10.1016/j.materresbull.2005.01.009
11. Fang Z, Tang K, Gao L, Wang D, Zeng S, Liu Q (2007) Facile and large-scale synthesis of single-crystalline manganese oxyhydroxide/oxide nanostructures. Mater Res Bull 42:1761–1768. https://doi.org/10.1016/j.materresbull.2006.11.025
12. Wang N, Guo L, He L, Cao X, Chen C, Wang R, Yang S (2007) Facile synthesis of monodisperse Mn_3O_4 tetragonal nanoparticles and their large-scale assembly into highly regular walls by a simple solution route. Small 3:606–610. https://doi.org/10.1002/smll.200600283
13. Cui X, Li Y, Sun G, Ma J, Zhang L, Ma RB (2014) Mn_3O_4 nano-sized crystals: rapid synthesis and extension to preparation of nano-sized $LiMn_2O_4$ materials. J Chem Sci 126:561–567. https://doi.org/10.1007/s12039-014-0592-1
14. Apte SK, Naik SD, Sonawane RS, Kale BB, Pavaskar N, Mandale AB, Das BK (2006) Nanosize Mn_3O_4 (Hausmannite) by microwave irradiation method. Mater Res Bull 41:647–654. https://doi.org/10.1016/j.materresbull.2005.08.028
15. Kamran U, Bhatti N, Iqbal M, Nazir A (2019) Green synthesis of metal nanoparticles and their applications in different fields: a review zeitschriftfür physikalische. Chemie 233(2019):1325–1349. https://doi.org/10.1515/zpch-2018-1238
16. Hoseinpour V, Ghaemi N (2018) Green synthesis of manganese nanoparticles: applications and future perspective–a review . J. Photochem. Photobiol B, Biol 189:234–243. https://doi.org/10.1016/j.jphotobiol.2018.10.022
17. Hatamifard A, Nasrollahzadeh M, Lipkowskib J (2015) Green synthesis of a natrolite zeolite/palladium nanocomposite and its application as a reusable catalyst for the reduction of organic dyes in a very short time. RSC Adv 5:91372–91381. https://doi.org/10.1039/C5RA18476B
18. Khodadadi B, Bordbar M, Nasrollahzade M (2017) Achillea millefolium L. extract mediated green synthesis of waste peach kernel shell supported silver nanoparticles: application of the nanoparticles for catalytic reduction of a variety of dyes in water. J Colloid Interface Sci 493:85–93. https://doi.org/10.1016/j.jcis.2017.01.012

19. Nasrollahzadeh M, Sajjadi M, Iravani S, Varma RS (2021) Green-synthesized nanocatalysts and nanomaterials for water treatment: current challenges and future perspectives. J Hazard Mater 401:123401. https://doi.org/10.1016/j.jhazmat.2020.123401
20. Bordbara M, Negahdara N, Nasrollahzadeh N (2018) Laser ablation assisted preparation of MnO_2 nanocolloids from waste battery cell powder: evaluation of physico-chemical, electrical, and biological properties. Sep Purif Technol 191:295–300
21. Prasad AS (2017) Green synthesis of nanocrystalline manganese (II, III) oxide. Mater Sci Semicond Process 71:342–347. https://doi.org/10.1016/j.mssp.2017.08.020
22. Asaikkutti A, Bhavan PS, Vimala KM, Karthik P (2016) Cheruparambath, Dietary supplementation of green synthesized manganese-oxide nanoparticles and its effect on growth performance, muscle composition and digestive enzyme activities of the giant freshwater prawn Macrobrachiumrosenbergii. J Trace Elem Med Biol 35:7–17. https://doi.org/10.1016/j.jtemb.2016.01.005
23. Sharma JK, Srivastava P, Ameen S, Akhtar MS, Singh G, Yadava S (2016) Azadirachtaindica plant-assisted green synthesis of Mn_3O_4 nanoparticles: excellent thermal catalytic performance and chemical sensing behavior. J Colloid Interface Sci 472:220–228. https://doi.org/10.1016/j.jcis.2016.03.052
24. Sreekala NG, Abdullakutty F, Bha B (2019) Green synthesis, characterization, and photo catalytic degradation efficiency of trimanganese tetroxide nanoparticle. Int J Nano Dimens 10:400–409
25. Beltrán-Debón R, Rull A, Rodríguez-Sanabria F et al (2011) Continuous administration of polyphenols from aqueous rooibos (Aspalathus linearis) extract ameliorates dietary-induced metabolic disturbances in hyperlipidemic mice. J Phytomed Phytomed 18:414–424. https://doi.org/10.1016/j.phymed.2010.11.008
26. Joubert E (1996) HPLC quantification of the dihydrochalcones, aspalathin and nothofagin in rooibos tea (Aspalathus linearis) as affected by processing. Food Chem 55:403–411. https://doi.org/10.1016/0308-8146(95)00166-2
27. Senthilkumar SR, Sivakumar T (2014) Green tea (camelliasinensis) mediated synthesis of zinc oxide (zno) nanoparticles and studies on their antimicrobial activities. Int J Pharm Pharm Sci 6:462–465. https://innovareacademics.in/journal/ijpps/Vol6Issue6/9715.pdf
28. McMurdie HF, Sullivan BM, Mauer FA (1950) High-temperature x-ray study of the system Fe_3O_4-Mn_3O_4. J Res Nat Bur Stand 45:35. https://doi.org/10.6028/jres.045.004
29. Gorbenko OY, Graboy IE, Amelichev VA, Bosak AA, Kaul AR, Güttler B, Svetchnikov VL, Zandbergen HW (2002) The structure and properties of Mn3O4 thin films grown by MOCVD. Solid State Commun 124:15. https://doi.org/10.1016/S0038-1098(02)00470-2
30. Sackey J, AkbariabMMorad M, Bashir AKH, Ndiaye NM, Matinise N, Maaza M (2021) Molecular dynamics and bio-synthesis of phoenix dactylifera mediated Mn_3O_4 nanoparticles: electrochemical application. J Alloys Compd 854:1569872. https://doi.org/10.1016/j.jallcom.2020.156987
31. Sone BT, Manikandan E, Gurib-Fakim A, Maaza M (2016) Single-phase α-Cr2O3 nanoparticles' green synthesis using Callistemon viminalis' red flower extract. Green Chem Lett Rev 9:85–90. https://doi.org/10.1080/17518253.2016.1151083
32. Julien CM, Massot M, Poinsignon C (2004) Lattice vibrations of manganese oxides part I periodic structures. Spectrochim Acta A60:689. https://doi.org/10.1016/S1386-1425(03)00279-8
33. Satomi K (1961) Oxygen Positional Parameters of Tetragonal Mn_3O_4. J Phys Soc Japan 16:258. https://doi.org/10.1143/JPSJ.16.258
34. Post JE (1999) Manganese oxide minerals: crystal structures and economic and environmental significance. Proc Natl Acad Sci USA 96:3447. https://doi.org/10.1073/pnas.96.7.3447
35. Kirillov SA, AleksandrovaVS LTV, Dzanashvili DI, Khainakov SA, García JR, Visloguzov NM, Pendelyuk OI (2009) Oxidation of synthetic hausmannite (Mn_3O_4) to manganite (MnOOH). J Mol Struct 928:89–94. https://doi.org/10.1016/S1386-1425(03)00279-8
36. Julien CM, Massot M (2003) Lattice vibrations of materials for lithium rechargeable batteries I. lithium manganese oxide spinel. Mater Sci Eng B 97:217–230. https://doi.org/10.1016/S0921-5107(02)00582-2
37. Buciuman F, Patcas F, Craciun R, Zahn DRT (1999) Vibrational spectroscopy of bulk and supported manganese oxides. Phys Chem Chem Phys 1:185. https://doi.org/10.1039/A807821A
38. Xu HY, Xu SH, Li XD, Wang H, Yan H (2006) Chemical bath deposition of hausmanniteMn$_3$O$_4$ thin films. Appl Surf Sci 252:4091. https://doi.org/10.1016/j.apsusc.2005.06.011
39. Chen ZW, Lai JKL, Shek CH (2005) Nucleation site and mechanism leading to growth of bulk-quantity Mn_3O_4 nanorods. Appl Phys Lett 86:181911. https://doi.org/10.1063/1.1923753
40. Zuo J, Xu C, Liu Y, Qian Y (1998) Crystallite size effects on the Raman spectra of Mn_3O_4. Nano Struct Mater 10:1331. https://doi.org/10.1016/S0965-9773(99)00002-1
41. Hu CC, Wu YT, Chang KH (2008) Low-temperature hydrothermal synthesis of Mn_3O_4 and MnOOH single crystals: determinant influence of oxidant. Chem Mater 20:2890–2894. https://doi.org/10.1021/cm703245k
42. Hu Y, Chen J, Xue X, Li T (2006) Synthesis of monodispersed single-crystal compass-shaped Mn_3O_4 via gamma-ray irradiation. Mater Lett 60:383. https://doi.org/10.1016/j.matlet.2005.08.056
43. Richter H, Wang ZP, Ley L (1981) The one phonon Raman spectrum in microcrystalline silicon. Solid State Commun 39:625. https://doi.org/10.1016/0038-1098(81)90337-9
44. Campbell IH, Fauchet PM (1986) The effects of microcrystal size and shape on the one phonon Raman spectra of crystalline semiconductors. Solid State Commun 58:739. https://doi.org/10.1016/0038-1098(86)90513-2
45. Jian Z, Cunyi X, Hou B, Wang C, Xie Y, Qian Y (1996) Raman Spectra of Nanophase Cr_2O_3. J Raman Spect 27:921. https://doi.org/10.1002/(SICI)1097-4555(199612)27:12%3c921::AID-JRS57%3e3.0.CO;2-L
46. Ford RB, Jackman GC, Allen GC (1984) An X-ray photoelectron spectroscopic investigation of the oxidation of manganese. Phil Mag 49:657. https://doi.org/10.1080/01418618408233293
47. Toufiq AM, Wang FP, Javed Q, Li Q, Li Y, Khan M (2014) Synthesis, characterization and photoluminescent properties of 3D nanostructures self-assembled with Mn_3O4 nanoparticles. Mater Express 4:258–262. https://doi.org/10.1166/mex.2014.1167
48. Toufiq AM, Wang F, Javed Q, Li Q, Li Y (2014) Hydrothermal synthesis of $Cu_{0.45}Mn_{0.55}O_2$ nanowhiskers: Structural characterizations and optical properties. Mater Lett 118:34. https://doi.org/10.1016/j.matlet.2013.12.038
49. Song L, Zhang S, Wu X, Wei Q (2012) Controlled synthesis and optical properties of 1D frog egg-like $Mn(IO_3)_2$/MnO_2 composite nanostructures with ultra-high aspect ratio. Chem Eng J 187:385. https://doi.org/10.1016/j.cej.2012.01.131
50. Giri A, Goswami N, Pal M, Myint MTZ, Al-Harthi S, Singha A, Ghosh B, Dutta J, Pal SK (2013) Rational surface modification of Mn_3O_4 nanoparticles to induce multiple photoluminescence and room temperature ferromagnetism. J Mater Chem C 1:1885–1895. https://doi.org/10.1039/c3tc00709j
51. Khan, Gilani AAH (2006) selective bronchodilatory effect of rooibos tea (Aspalathus linearis) and its flavonoid. Chrysoeriol Eur J Nutr 45:463–469. https://doi.org/10.1007/s00394-006-0620-0

52. Matinise N, Fuku XG, Kaviyarasu MN, Maaza M (2017) ZnO nanoparticles via Moringa oleifera green synthesis: physical properties and mechanism of formation. Appl Surf Sci 406:339–347. https://doi.org/10.1016/j.apsusc.2017.01.219
53. Ismail E, Khenfouch M, Dhlamini M, Dube S, Maaza M (2017) Green palladium and palladium oxide nanoparticles synthesized via Aspalathus linearis natural extract. J Alloys Compd 695:3632–3638. https://doi.org/10.1016/j.jallcom.2016.11.390
54. Ezhilarasi AA, Vijaya JJ, Kaviyarasu K, Maaza M, Ayeshamariam A, Kennedy LJ (2016) Green synthesis of NiO nanoparticles using Moringa oleifera extract and their biomedical applications: Cytotoxicity effect of nanoparticles against HT-29 cancer cells. J PhotochPhotobio B 164:352–360. https://doi.org/10.1016/j.jphotobiol.2016.10.003
55. Sone BT, Diallo A, Fuku XG, Gurib-Fakim A, Maaza M (2018) Biosynthesized CuO nano-platelets: physical properties and enhanced thermal conductivity nanofluidics. Arab J Chem 13:160–170. https://doi.org/10.1016/j.arabjc.2017.03.004
56. Diallo A, Mothudi M, Manikandan E, Maaza M (2016) Luminescent Eu_2O_3 nanocrystals by Aspalathus linearis' extract: structural and optical properties. J of Nanophotonics 10:026010. https://doi.org/10.1117/1.JNP.10.026010
57. Diallo A, Manikandan E, Rajendran V, Maaza M (2016) Physical & enhanced photocatalytic properties of green synthesized SnO2 nanoparticles via Aspalathus linearis. J Alloys Compd 681:561–570. https://doi.org/10.1016/j.jallcom.2016.04.200
58. Diallo A, Doyle TB, Mothudi BM, Manikandan E, Rajendran V, Maaza M (2017) Magnetic behavior of biosynthesized Co_3O_4 nanoparticles. J Magn Magn Mater 425:251–255. https://doi.org/10.1016/j.jmmm.2016.10.063
59. Diallo A, Kaviyarasu K, Ndiaye S, Mothudi BM, Ishaq A, Rajendran V, Maaza M (2018) Structural, optical, and photocatalytic applications of biosynthesized NiO nanocrystals. Green Chem Lett Rev 11:166–175. https://doi.org/10.1080/17518253.2018.1447604
60. Thema FT, Manikandan E, Dhlamini MS, Maaza M (2015) Green synthesis of ZnO nanoparticles via Agathosmabetulina natural extract. MaterLett 161:124–127. https://doi.org/10.1016/j.matlet.2015.08.052
61. Khalil AT, Ovais M, Ullah I, Ali M, Shinwari ZK, Hassan D, Maaza M (2017) Sageretiathea (Osbeck.) modulated biosynthesis of NiO nanoparticles and their in vitro pharmacognostic, antioxidant and cytotoxic potential. Artif Cell Nanomed B 46:838–852. https://doi.org/10.1080/21691401.2017.1345928
62. Kaviyarasu K, Magdalane CM, Anand K, Manikandan E, Maaza M (2015) Synthesis and characterization studies of MgO: CuO nanocrystals by wet-chemical method. Spectrochim Acta A Mol BiomolSpectrosc 142:405–409. https://doi.org/10.1016/j.saa.2015.01.111
63. Khamlich S, Manikandan E, Ngom JS, Nemraoui O, Zorkani I et al (2011) Synthesis, characterization, and growth mechanism of α-Cr2O3 monodispersed particles. J Phys Chem Solids 72:714–718. https://doi.org/10.1016/j.jpcs.2011.02.015
64. Khenfouch M, Baïtoul M, Maaza M (2012) White photoluminescence from a grown ZnO nanorods/graphene hybrid nanostructure. Opt Mater 34:1320–1326. https://doi.org/10.1016/j.optmat.2012.02.005
65. Magdalane CM, Kaviyarasu K, Matinise N et al (2018) Evaluation on La_2O_3 garlanded ceria heterostructured binary metal oxide nanoplates for UV/visible light induced removal of organic dye from urban wastewater. South S Afr J Chem Eng 26:49–60. https://doi.org/10.1016/j.sajce.2018.09.003
66. KarthikS SP, Balu KS, Suriyaprabha R, Rajendran V, Maaza M (2017) Acalypha indica–mediated green synthesis of ZnO nanostructures under differential thermal treatment: Effect on textile coating, hydrophobicity, UV resistance, and antibacterial activity. Adv Powder Technol 28:184–3194. https://doi.org/10.1016/j.apt.2017.09.033
67. Kaviyarasu K, Magdalane CM, Manikandan E, Jayachandran M et al (2015) Well-aligned graphene oxide nanosheets decorated with zinc oxide nanocrystals for high performance photocatalytic application. Int J Nanosci 14(03):1550007. https://doi.org/10.1142/S0219581X15500076
68. Khalil AT, Ovais M, Ullah I, Ali M, Shinwari ZK, Khamlich S, Maaza M (2017) Mediated synthesis of zinc oxide nanoparticles and its biological applications. Nanomedicine 12:1767–1789
69. Ekambaram S, Patil KC, Maaza M (2005) Synthesis of lamp phosphors: facile combustion approach. J J Alloys Compd 393:81–92. https://doi.org/10.1016/j.jallcom.2004.10.015
70. Ekambaram S, Maaza M (2005) Combustion synthesis and luminescent properties of Eu3+-activated cheap red phosphors. J Alloys Compd 395:132–134. https://doi.org/10.1016/j.jallcom.2004.09.075
71. Mayedwa N, Mongwaketsi N, Khamlich S, Kaviyarasu K, Matinise N et al (2018) Green synthesis of nickel oxide, palladium and palladium oxide synthesized via Aspalathus linearis natural extracts: physical properties and mechanism of formation. Appl Surf Sci 446:266–272. https://doi.org/10.1016/j.apsusc.2017.12.116